Hydrometallurgy 223 (2024) 106221

Contents lists available at ScienceDirect

Hydrometallurgy

journal homepage: www.elsevier.com/locate/hydromet

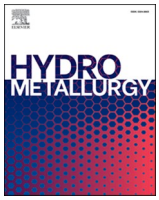

Selective separation of aluminum, silicon, and titanium from red mud using oxalic acid leaching, iron precipitation and pH adjustments with calcium carbonate

Wanyan Li [a,b], Ning Wang [a], Fanghai Lu [c], Hongyun Chai [d], Hannian Gu [a,b,*]

[a] Key Laboratory of High-temperature and High-pressure Study of the Earth's Interior, Institute of Geochemistry, Chinese Academy of Sciences, Guiyang 550081, China
[b] University of Chinese Academy of Sciences, Beijing 100049, China
[c] School of Materials and Energy Engineering, Guizhou Institute of Technology, Guiyang 550003, China
[d] SPIC Zunyi Industrial Development Co., Ltd., Zunyi 564300, China

ARTICLE INFO

Keywords:
Red mud
Oxalic acid
Selective separation
Aluminum
Titanium concentrate

ABSTRACT

Red mud discharged from alumina production is a valuable metal resource of great importance in the context of the requirement to reduce the impact of mining on the environment and resource consumption. The efficient dissolution of iron from red mud by oxalic acid has been reported. Although the concentrations of aluminum, silicon, and titanium were also high in the red mud-oxalic acid leachate after iron precipitation, they have received little attention. The present study aims to recover aluminum, silicon, and titanium from red mud-oxalic acid leachate after the precipitation of iron. The leaching efficiencies of aluminum, silicon, and titanium in 1.0 mol/L oxalic acid at 80 °C, reached 63–75% after 2 h. Sodium hydroxide, calcium oxide, and calcium carbonate were chosen to adjust the pH of the oxalic acid leachate, and the effective separation of silicon and titanium from the oxalic acid leachate could be achieved at pH 4.0 by stepwise separation using calcium carbonate. A silicon dioxide primary product with a purity of 70.8% was obtained in addition to the aluminum hydroxide primary product. The stepwise selective separation of aluminum, silicon, and titanium from red mud-oxalic acid leachate could assist the values recovery and simultaneously minimize environmental hazards of the acidic leachate.

1. Introduction

Red mud (RM), also known as bauxite residue, is an alkaline industrial solid waste derived during the Bayer process for extracting alumina from bauxite ores (Borra et al., 2016). Generally, the production of 1 ton of alumina generates approximately 1–1.5 tons of RM depending on the raw material quality and process parameters (Taneez and Hurel, 2019; Zhang et al., 2021; Zhou et al., 2023). With the increasing demand for alumina production, the worldwide discharge of RM increased to approximately 200 million tons annually (Xue et al., 2019). Since <5% of RM has been reused (Barca et al., 2022), the stockpiled RM has brought environmentally unacceptable impacts (Agrawal and Dhawan, 2021; Liu et al., 2021; Li et al., 2022b). Meanwhile, RM is considered as a potential polymetallic source as it contains a variety of valuable metals in appreciable quantities, such as aluminum, iron, titanium, and rare earth elements (REEs) (Liu and Naidu, 2014; Rivera et al., 2018; Qu et al., 2022). To extract and recover these valuable components from RM, researchers around the globe have carried out diverse research programs, chiefly including pyrometallurgical and hydrometallurgical approaches. Pyrometallurgical methods usually involve carbothermal reduction and magnetic separation to obtain Fe components (Habibi et al., 2021; Wan et al., 2021; Yu et al., 2022), which can achieve high recovery efficiencies but require high-temperature treatment and high energy consumption. The hydrometallurgical methods were suited for extraction from complex structured RM through mineral acids or organic acids leaching and extraction process (Zhu et al., 2015; Agrawal and Dhawan, 2020).

In particular, organic acids, in some occasions, could exhibit greater leaching efficiencies of metals from inert minerals in RM compared to leaching efficiencies with mineral acids. This is because of the dual effects of metal bond destabilization by charge transfers and the chelation of the metal and organic ligands (Gräfe et al., 2011; Liu and Li, 2015;

* Corresponding author at: Key Laboratory of High-temperature and High-pressure Study of the Earth's Interior, Institute of Geochemistry, Chinese Academy of Sciences, Guiyang 550081, China.
E-mail address: guhannian@vip.gyig.ac.cn (H. Gu).

https://doi.org/10.1016/j.hydromet.2023.106221
Received 30 June 2023; Received in revised form 9 October 2023; Accepted 9 October 2023
Available online 10 October 2023

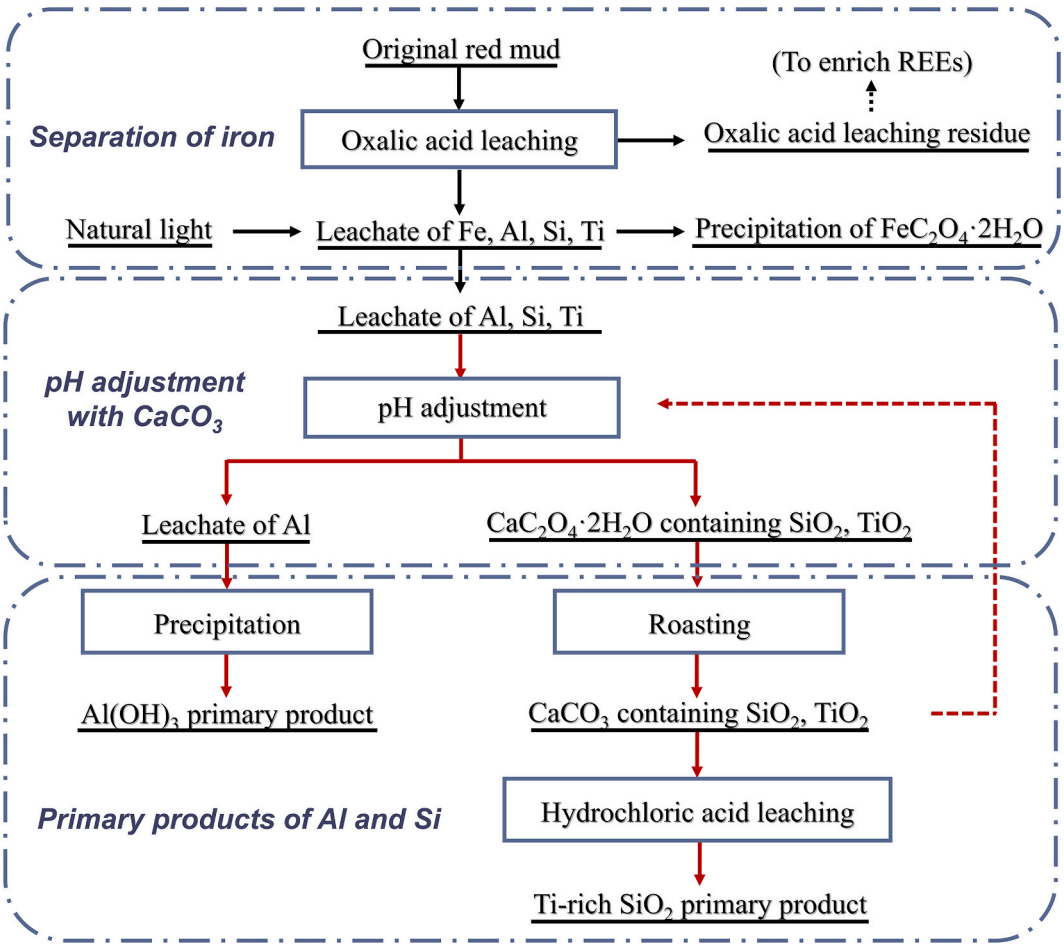

Fig. 1. Experimental flowsheet of stepwise separation of Al, Si, and Ti from RM.

Panda et al., 2021). Taking oxalic acid as an example, the previous studies suggested that oxalic acid leaching was effective to dissolve Fe from RM as soluble ferric oxalate, and then ferrous oxalate was separated by precipitation (Agrawal and Dhawan, 2022; Li et al., 2022a). This process was attributed to the high acid strength, the strong coordination effect, and the reducing power of oxalic acid (Ambikadevi and Lalithambika, 2000; Tanvar and Mishra, 2021). When RM was treated with oxalic acid, the Fe extraction efficiency could achieve 96% in the form of ferric oxalate complex, and then β-$FeC_2O_4·2H_2O$ could be separated after the reduction catalysed by UV irradiation (Yu et al., 2012) or natural light (Gu et al., 2017). The ferric oxalate in the pregnant leach solution could also be reduced into $FeC_2O_4·2H_2O$ precipitate by adding iron scraps (Yang et al., 2015). Moreover, the ferrous oxalate product was a precursor for preparing sodium ferrate (Na_2FeO_4), and this was shown to be a potential route for preparing high value-added Fe-containing compounds from RM (Gu et al., 2017). In addition, it was observed that REEs were released from the Fe-containing minerals forming REE-oxalates when RM was subjected to oxalic acid leaching. These REE-oxalates remained and enriched in the leach residue due to their low solubilities (Li et al., 2022a). Subsequently, REEs could be selectively leached with dilute sulfuric acid (Li et al., 2022a). Therefore, there were several advantages of using oxalic acid to dissolve Fe from RM, such as preparing various Fe-containing products and enriching REEs in the leach residue.

However, the oxalic acid dissolution process for iron recovery was restricted by the relatively high cost of oxalic acid, and recycling/reduction of oxalic acid in the process was considered as a means of offsetting partial cost (Yang et al., 2016). It deserves to be mentioned that a large proportion of Al, Si, and Ti were also dissolved in the oxalic acid leaching process, and these elements remained in the leachate after $FeC_2O_4·2H_2O$ was precipitated which also deserved to be recovered. The high extraction efficiency of Al was determined during the oxalic acid leaching process of RM (Yang et al., 2015; Ujaczki et al., 2019; Huang et al., 2021; Tanvar and Mishra, 2021). Thereinto, Huang et al. (2021) attempted to recover Al from the Fe-removed oxalic acid leachate with aqueous ammonia and reused oxalic acid by crystallization after evaporation. In addition to Al with a high leaching efficiency, Si and Ti were also co-dissolved in oxalic acid (Liu and Li, 2015; Liu et al., 2022). The comprehensive recovery of these metal products would make the oxalic acid leaching process more cost-effective and would avoid wasting these valuable resources. However, few studies investigated the recovery of Al, Si, and Ti in the RM-oxalic acid leachate and only concluded that they were undesirable elements during the Fe dissolution process. Therefore, a recovery process of Al, Si, and Ti from the Fe-removed oxalic acid solution should be developed.

This work aims to investigate the selective extraction of Al, Si, and Ti from the Fe-removed oxalic acid leachate of RM through a series of pH-adjusting experiments using NaOH, CaO, and $CaCO_3$. The aim is to propose a stepwise solution separation process involving pH adjustment and recycling the precipitate. The effects of NaOH, CaO, and $CaCO_3$ as pH adjusters on the selective extraction of Al, Si, and Ti from the oxalic acid leachate were evaluated by comparing the elemental concentration of the Fe-removed oxalic acid leachate and by characterizing the elemental contents of precipitates. The innovative stepwise recovery route would probably be a potential way to achieve extraction of elements and comprehensive utilization of RM-oxalic acid leachate while reducing chemical consumption.

2. Materials and method

2.1. Materials and reagents

The RM sample used in this study was collected from an alumina refinery in Qingzhen, Guizhou province, China. The fresh RM sample was in the form of small agglomerates after natural drying. Upon arrival in the laboratory, the RM sample was dried at 100 °C to achieve a constant weight. Prior to characterization and leaching experiments, the dried RM sample was pulverized and screened to <75 μm to ensure a uniform particle size distribution (Li et al., 2022a).

Oxalic acid of analytical grade (≥ 99.5 wt%) purchased from Tianjin Yongda Chemical Industrial Co., Ltd. was used for RM batch leaching experiments. Hydrochloric acid with guaranteed reagent grade (36.0–38.0 wt/v%) was used to wash the $CaCO_3$ precipitates. Analytical grade reagents of sodium hydroxide (NaOH ≥99 wt%), calcium oxide (CaO ≥ 97 wt%), and calcium carbonate ($CaCO_3$ ≥ 99 wt%) were applied for adjusting pH of the Fe-removed leachate. Additionally, all the solutions used in the experiments were prepared with deionized water.

2.2. Experimental procedure

The flowsheet shown in Fig. 1 involves three main operations: (i) oxalic acid leaching of RM to obtain an iron product and a REE-rich residue (Li et al., 2022a), (ii) pH adjustment for the Fe-removed leachate to precipitate Si and Ti, and (iii) production of $Al(OH)_3$ and SiO_2 (with Ti entrapped), as the two primary products. Fig. 1 also depicts the recycling of $CaC_2O_4{\cdot}2H_2O$ process to enrich SiO_2 and TiO_2. The following experiments are mainly based on the flowsheet.

2.2.1. Oxalic acid leaching and Fe separation

Batch oxalic acid leaching experiments were performed under the following procedure. A 250 mL three-neck flask was placed in a thermostated water bath (THZ-82A) at a certain temperature. The timer was started after adding the solid, with a stirring speed of 200 rpm. After filtration, the deionized water used to rinse the solid was added to the leachate and the volume was adjusted.

Leaching tests were carried out with oxalic acid by varying several parameters, i.e., acid concentration, leaching temperature, and liquid-to-solid ratio (L/S ratio). The concentration trial was carried out under the condition of oxalic acid concentrations of 0.5, 1.0, and 1.5 mol/L, L/S ratio of 15 mL/g, reaction time of 2 h, and leaching temperature of

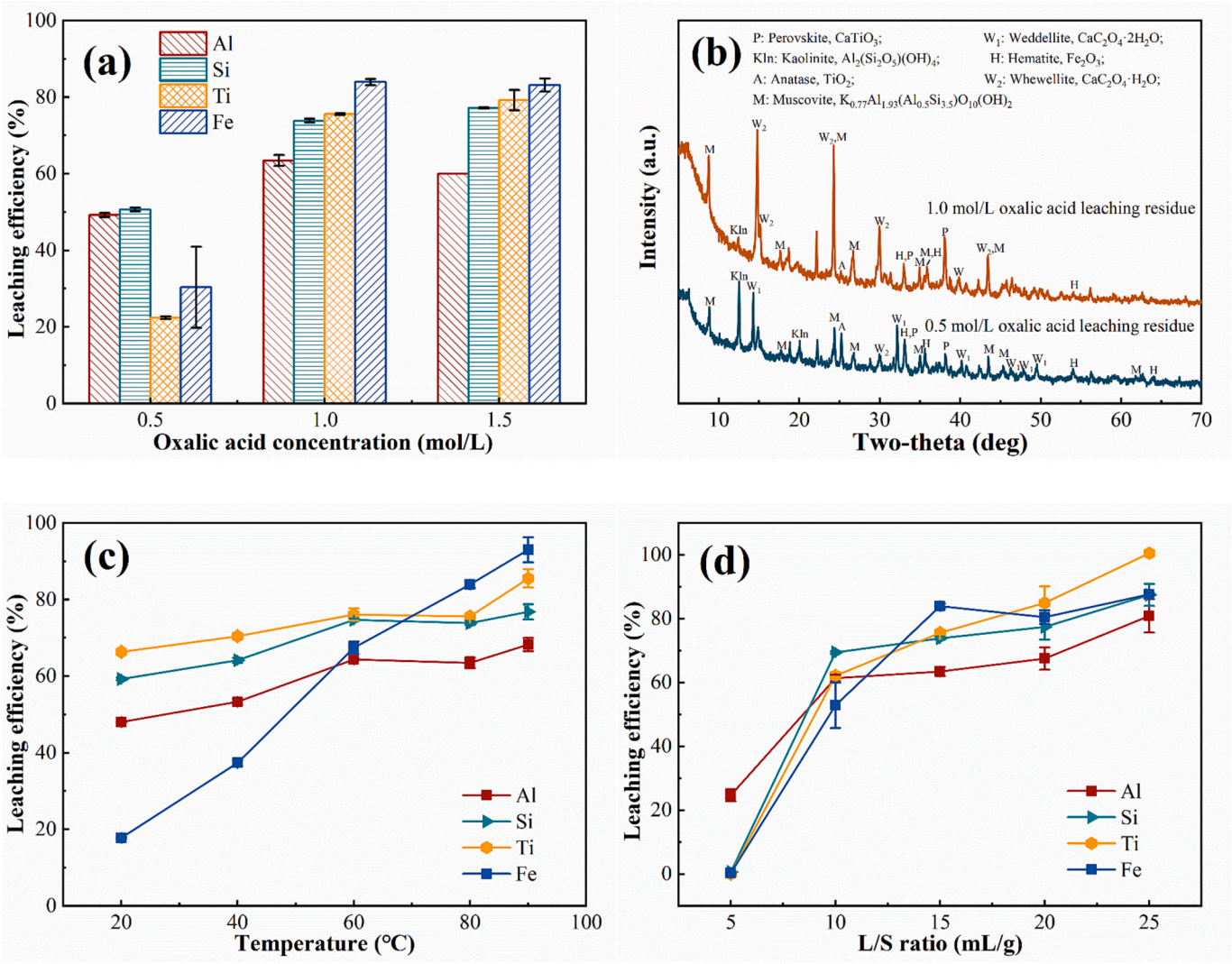

Fig. 2. Effects of different parameters on leaching efficiencies of Fe, Al, Si, and Ti from RM with changes in (a) oxalic acid concentrations, (c) temperatures, (d) L/S ratios; (b) XRD patterns of 0.5 mol/L and 1.0 mol/L oxalic acid leach residues (general leaching conditions: 1 mol/L oxalic acid at 80 °C for 2 h with L/S ratio of 15 mL/g, unless stated in each figure).

80 °C. The effect of leaching temperature was evaluated at 20, 40, 60, 80, and 90 °C for 2 h using 1.0 mol/L oxalic acid with the L/S ratio of 15 mL/g. The L/S ratio trial was carried out with L/S ratio of 5, 10, 15, 20, and 25 mL/g using 1.0 mol/L oxalic acid concentration at a leaching temperature of 80 °C for 2 h. Each trial of oxalic acid leaching was conducted twice to obtain the average results.

The filtrate from the RM-oxalic acid leachate was irradiated by sunlight at room temperature until Fe was precipitated as ferrous oxalate dihydrate. Subsequently, the Fe-removed oxalic acid leachate was obtained after filtering the ferrous oxalate. In the oxalic acid leaching process, the leaching efficiencies of Al, Si, and Ti can be expressed by Eq. (1), while, the leaching efficiency of Fe is estimated by the Fe content in ferrous oxalate according to Eq. (2):

$$\eta_i = \frac{c_i \bullet V}{0.001 \bullet c_{i0} \bullet m_0} \times 100\% \quad (1)$$

$$\eta_{Fe} = \frac{m_{FeC_2O_4\cdot 2H_2O} \times \frac{M_{Fe}}{M_{FeC_2O_4\cdot 2H_2O}}}{m_0 \times c_{Feo}} \times 100\% \quad (2)$$

where η_i and η_{Fe} are the leaching efficiency of the element i and Fe, respectively; c_i is the concentration of the element i in the leachate (mg/L), V is the volume of the leachate (L), m_{Fe} is the mass of $FeC_2O_4{\cdot}2H_2O$ precipitate (g), c_{i0} is the content of the element i in the RM (%), c_{Fe0} is the content of the element Fe in the RM (%), m_0 is the mass of RM (g), and M_{Fe} and $M_{FeC_2O_4\cdot 2H_2O}$ are the molar masses of Fe and $FeC_2O_4{\cdot}2H_2O$ (g/mol), respectively.

2.2.2. Al and Si separation

The initial pH of the Fe-removed oxalic acid leachate was 0.82 ± 0.04. In this test, the separation behavior of Al and Si was evaluated by adjusting the pH of 100 mL aliquots of the Fe-removed oxalic acid leachate by adding NaOH, CaO, or $CaCO_3$. A solution of 4.0 mol/L NaOH was used to adjust the pH values from 0.82 to 8.0. The effects of pH adjustments from 0.82 to a lower pH of 5.0 were investigated by adding CaO or $CaCO_3$. Each test of the pH adjustment was conducted in triplicate and the results presented were averaged.

In the pH-adjusted process, the retention efficiency (η_j) of elements (j = Al, Si, or Ti) in the leachate as a percentage of the initial concentration of j in Fe-removed oxalic acid leachate can be calculated according to Eq. (3):

$$\eta_j = \frac{c_{j2} \bullet V_{j2}}{c_{j1} \bullet V_{j1}} \times 100\% \quad (3)$$

where V_{j1} and V_{j2} are the volumes of the leachate before and after pH adjustment (L), respectively, and c_{j1} and c_{j2} are the concentrations of the element j in the leachate before and after pH adjustment (mg/L), respectively.

2.2.3. The primary products of Si, Ti, and Al

The precipitate produced from the Fe-removed oxalic acid leachate, after adjusting pH to 4.0 using $CaCO_3$, was filtered at pH 4.0 and roasted at 520 °C for 2 h. The roasted precipitate was then added for the next pH adjustment with 100 mL of Fe-removed oxalic acid leachate until this recirculation process was repeated 3 times. Then the roasted precipitate was washed with 0.5 mol/L dilute HCl to obtain SiO_2 of high purity. Additionally, the filtered Al-enriched leachate was used to precipitate amorphous $Al(OH)_3$ after impurity removal by NaOH.

2.3. Characterization methods

The variation of $C_2O_4^{2-}$ content in the Fe-removed leachate was determined by titrating with a standard potassium permanganate solution (Yang et al., 2016). The compositions of major elements in the digested solid samples were determined using an inductively coupled plasma optical emission spectrometer (ICP-OES, Agilent 5110, USA). The microstructure of the solid samples was studied by scanning electron microscopy (SEM, JSM-7800F, Japan). By using an X-ray diffractometer (XRD, PANalytical Empyrean, the Netherlands) with Cu Kα radiation at the 2θ range of 5–70°, the phase compositions of precipitates were identified. The SiO_2 in solid samples was measured by X-ray fluorescence spectroscopy (XRF, PANalytical PW2424, the Netherlands). The pH values of solutions in this study were measured using a pH meter (PHS-3C).

3. Results and discussion

3.1. Oxalic acid leaching process

Previous work has revealed the optimum leaching conditions for Fe recovery from RM using oxalic acid (Yu et al., 2012). The effect of oxalic acid concentration on RM dissolution was investigated with a L/S ratio of 15 mL/g at 80 °C with stirring for 2 h. The results are shown in Fig. 2a. The Fe dissolution reached 30.3% at 0.5 mol/L oxalic acid, and increased to 83.9% at 1.0 mol/L oxalic acid. Similar dissolution trends were observed for Al, Si, and Ti. Specifically, the leaching efficiency of Ti in 0.5 mol/L oxalic acid was low, which was attributed to the stability of Ti-containing minerals in RM, such as anatase and rutile at low acid concentrations (Pepper et al., 2016; Deng et al., 2017). The XRD patterns of oxalic acid leach residues produced in 0.5 mol/L and 1.0 mol/L are depicted in Fig. 2b. The peaks of calcium oxalate ($CaC_2O_4{\cdot}nH_2O$) were enhanced with the increasing oxalic acid concentration, and the peaks of Fe-, Al-, Si-, and Ti-bearing phases were weakened or disappeared. However, no significant increase in the leaching efficiencies of elements was observed after a further increase of oxalic acid concentration from 1.0 to 1.5 mol/L. The results indicated that 1.0 mol/L oxalic acid was suitable for efficient leaching of Fe from RM, consistent with previous studies (Gu et al., 2017). Results from this study in Fig. 2 demonstrated that >63% of Al and 73% of Ti and Si in RM were also dissolved in the process.

Fig. 2c presents the effect of various leaching temperatures with 1.0 mol/L oxalic acid to leach RM at L/S ratio of 15 mL/g for 2 h. As reported in previous studies (Yu et al., 2012), the increase in temperature from 20 to 60 °C significantly increased the Fe dissolution efficiency, as it promotes ionic activity in the solution (Pepper et al., 2016). However, differing from Fe, as shown in Fig. 2c, Al, Si, and Ti exhibited similar dissolution tendencies and showed moderate increases of dissolution at the same temperature range. Even at a low temperature of 20 °C, 48–66% of these elements could be dissolved (Ti > Si > Al), but their dissolution efficiencies were surpassed by Fe when the reaction temperature reached 80 °C. At a reaction temperature of 90 °C, leaching efficiencies of Fe, Al, Si, and Ti reached 93, 68, 77, and 86%, respectively, implying that the oxalic acid leaching at this condition for Fe recovery could co-dissolve appreciable amounts of Al, Si, and Ti.

The leaching efficiencies of Fe, Al, Si, and Ti all showed rapid increases with the L/S ratio changing from 5 to 10 mL/g, indicating that the amount of oxalic acid was insufficient at the L/S ratio of 5 mL/g. According to literature (Yu et al., 2012), L/S ratio of 10 mL/g was selected to recover Fe from RM, while, L/S ratio of 15 mL/g was used to

Table 1
Concentrations of major elements and initial pH of the Fe-removed leachate.

Composition	Al	Si	Na	Fe	Ti	K	Mg	Ca	pH
Content (mg/L)	4195	3155	1730	290	885	333	310	146	0.82

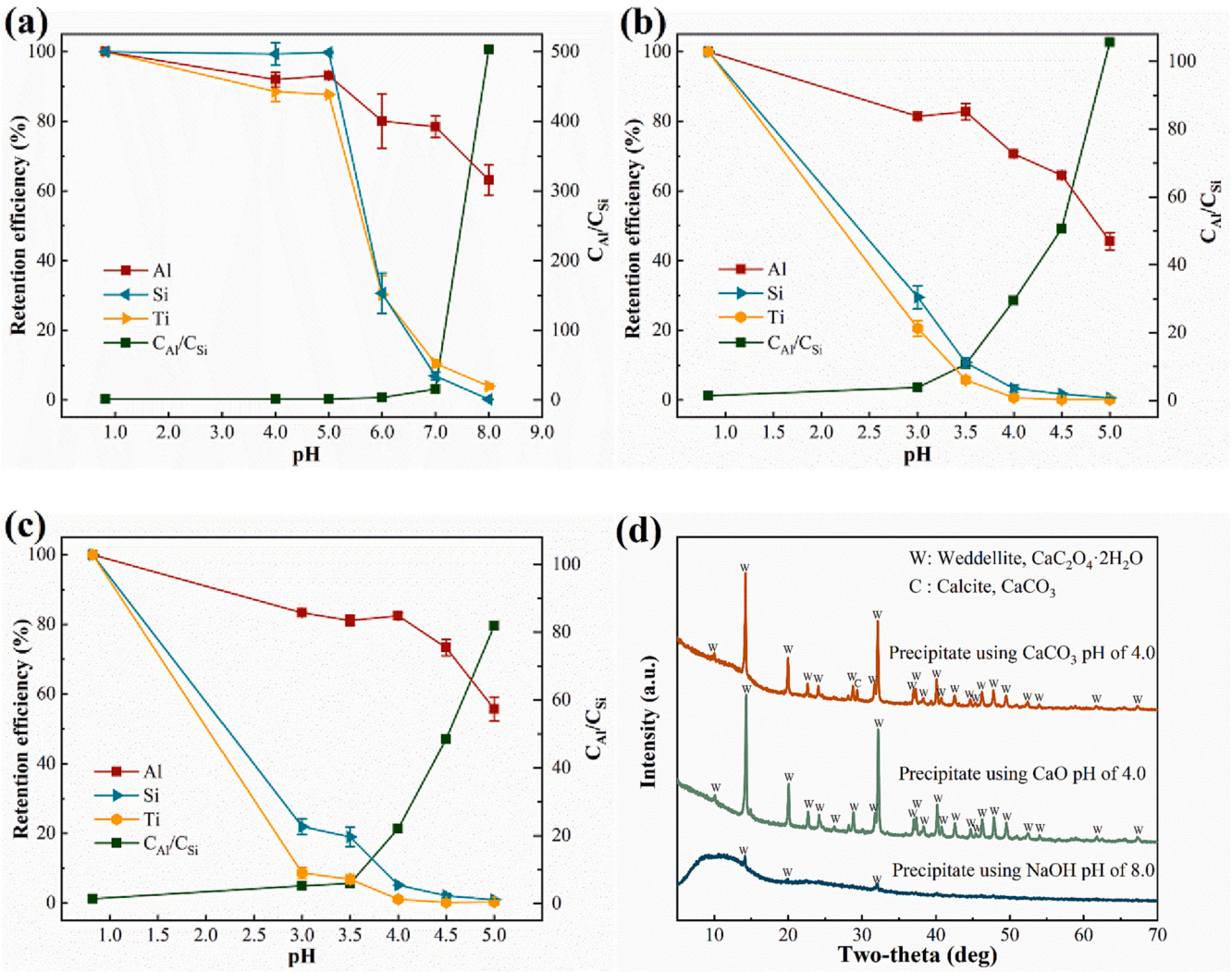

Fig. 3. Effects of pH on the retention efficiencies (%) of Al, Si, and Ti in the Fe-removed leachate when using (a) NaOH, (b) CaO, and (c) $CaCO_3$ for pH adjustment, respectively, and (d) the XRD patterns of precipitates (retention efficiency was calculated using Eq. 3).

prepare leachate for subsequent Al, Si, and Ti separation. Based on the results in Fig. 2, the leaching efficiencies of Al, Si, and Ti could reach 63.5, 73.9, and 75.6%, respectively, at the condition of 1.0 mol/L oxalic acid with L/S ratio of 15 mL/g at 80 °C for 2 h. These large quantities of Al, Si, and Ti in the Fe-removed leachate justify the efforts for their recovery described below.

To prepare Fe-removed leachate, RM-oxalic acid leach solution obtained under the above-stated conditions of 1.0 mol/L oxalic acid, L/S ratio of 15 mL/g, at 80 °C for 2 h, was filtered after irradiation to sunlight. The Fe-removed leachate was used for subsequent Al, Si, and Ti separation investigations, and the elemental concentrations of the Fe-removed leachate are shown in Table 1. The concentration of Al was as high as 4195 mg/L followed by that of Si. The leachate also contained high Na content because the Na-phases in RM could be easily dissolved when subjected to acid treatment (Xue et al., 2019; Lyu et al., 2021). In addition to Al, Si, and Na, the leachate contained Ti with a concentration of 885 mg/L and $C_2O_4^{2-}$ with a concentration of 0.51 mol/L. While Al and Ti exist in the form of oxalate complexes, Si primarily exists as silicate in RM which could dissolve as orthosilicate or orthosilicic acid (H_4SiO_4) (Milne et al., 2014).

In general, the precipitation of metal ions as hydroxides is facilitated by increasing pH (Lee and Saunders, 2003). To raise the leachate pH, NaOH, CaO, and $CaCO_3$ were successively tested and compared to investigate the separation behavior of elements.

3.2. Effect of pH adjustment to 8.0 using NaOH

A solution of 4.0 mol/L NaOH was used to adjust the leachate pH. The experimental results are shown in Fig. 3a. Raising pH from 0.82 to 5.0, most of Al, Si, and Ti remained in the leachate because these elements could dissolve at high pH (Gräfe et al., 2011; Huang et al., 2016). Subsequently, increasing pH from 5.0 to 8.0 resulted in significant decreases in the concentration of Si and Ti. The polymerization of H_4SiO_4 was catalysed by the change in pH which led to the precipitation of SiO_2 gel as presented in Eq. (4) (Wilhelm and Kind, 2015; Li et al., 2021). The precipitates were amorphous colloids as depicted in Fig. 3d. Formation and precipitation of SiO_2 gel induced reduction of Al concentration probably by adsorption behavior, thus the retention of Al in the leachate was only approximately 60% at pH 8.0 (Fig. 3a). The SEM image of SiO_2 particles shown in Fig. 4a suggested that the precipitated SiO_2 particles always mixed with Ti and Al, implying a weak separation effect was achieved. Consequently, the separation of Al, Si, and Ti was infeasible through a simple increase in the leachate pH using NaOH, and the effect of the $C_2O_4^{2-}$ anion in the leachate should be taken into consideration.

$$H_4SiO_4 \rightarrow SiO_2(gel) + 2H_2O \quad (4)$$

3.3. Effect of pH adjustment to 4.0 using CaO

To investigate the effect of $C_2O_4^{2-}$ in the leachate, powdered CaO was

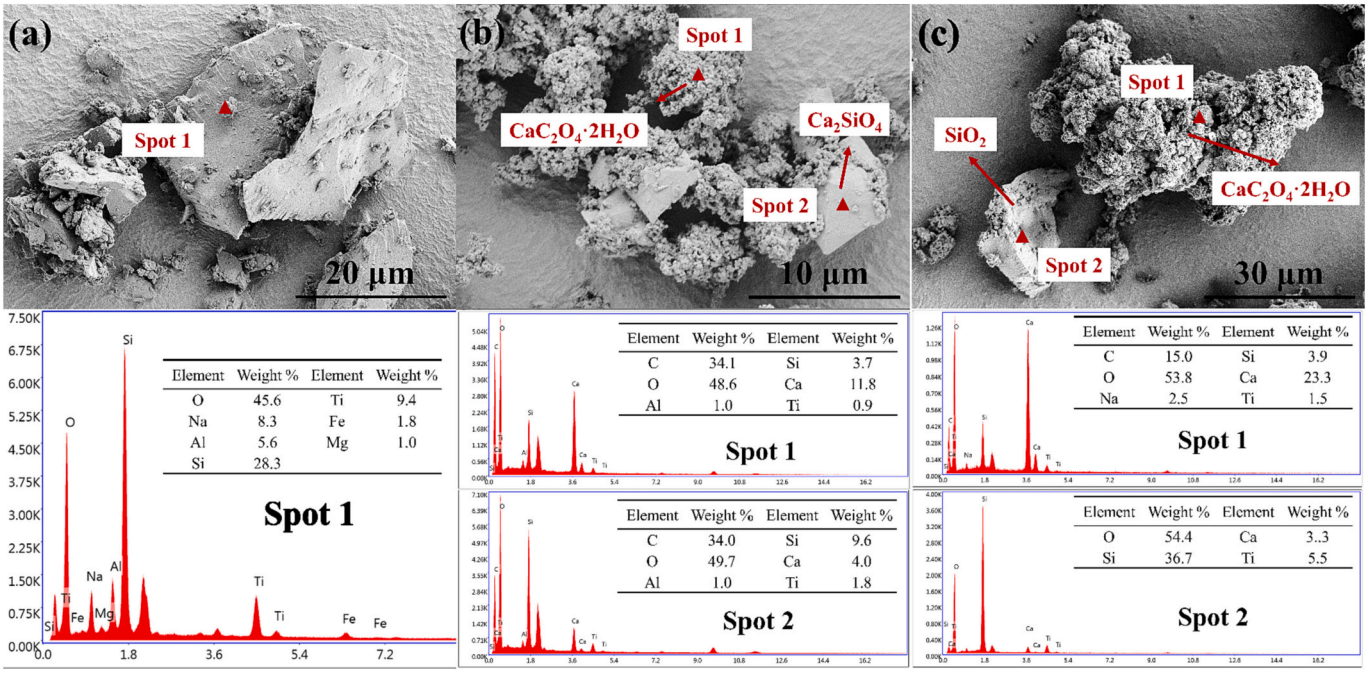

Fig. 4. SEM images and EDS analysis of precipitates obtained at the condition of (a) pH at 8.0 using NaOH, (b) pH at 4.0 using CaO, and (c) pH at 4.0 using $CaCO_3$.

Table 2
The contents of elements in the leachates after different pH adjustments.

Description	Content (mg/L)							
	Al	Si	Na	Fe	Ti	K	Mg	Ca
Fe-removed leachate at pH 0.82	4195	3155	1730	290	885	333	310	146
After adding NaOH to adjust pH to 8.0	2910	6	12,283	133	38	245	227	5
After adding CaO to adjust pH to 4.0	3473	122	1458	139	7	302	349	802
After adding $CaCO_3$ to adjust pH to 4.0	3965	140	1525	179	65	298	338	955

added to increase the pH and to reduce the $C_2O_4^{2-}$ concentration. The results are illustrated in Fig. 3b. The retention (%) of Si and Ti in the leachate significantly decreased when the pH was increased to 3.0. At this point, the retention of Al was still 80%, and much higher than that of Si and Ti. At pH 4.0, the retention efficiencies of both Si and Ti were <4%. The reaction of CaO in the leachate might experience three stages to establish equilibrium, summarized as Eqs. (5–7). As indicated in Table 2, a small fraction of Ca^{2+} equilibrated with $C_2O_4^{2-}$ in the leachate at pH 4.0. The reactions with CaO were much slower, compared to those with NaOH, resulting in H_4SiO_4 in the leachate combined with Ca^{2+} forming Ca_2SiO_4 precipitate instead of dehydration forming SiO_2 gel (Kong et al., 2017). As can be seen from Fig. 4b, the species of precipitation generated using CaO were octahedral-shaped Ca_2SiO_4 particles with large agglomerates of $CaC_2O_4·2H_2O$. At pH 4.0, Si and Ti were largely precipitated, and 70.7% of Al remained in the solution.

$$CaO + H_2C_2O_4 + H_2O \rightarrow CaC_2O_4·2H_2O \quad (5)$$

$$CaO + 2H_2C_2O_4 \rightarrow Ca(HC_2O_4)_2 + H_2O \quad (6)$$

$$2Ca^{2+} + H_4SiO_4 \rightarrow Ca_2SiO_4 + 4H^+ \quad (7)$$

3.4. Effect of pH adjustment to 4.0 using $CaCO_3$

The use of powdered $CaCO_3$ to adjust pH can achieve faster chemical reaction/equilibration and removal of Si and Ti from the leachate. Fig. 3c presents the influence of pH on Si and Ti precipitation from the leachate and shows that there has been a sharp decline in retention efficiencies of Si and Ti to 5.2% and 1.1%, respectively, with the increase in pH from 0.82 to 4.0, while Al retention remained at 82.5%. Oxalic acid dissociated into H^+ and $HC_2O_4^-$ at pH < 2.0, and $HC_2O_4^-$ further dissociated as $C_2O_4^{2-}$ at pH > 4.0 (Tanvar and Mishra, 2021); $CaCO_3$ could react with $H_2C_2O_4$ directly and with the oxalate anions in the leachate to precipitate $CaC_2O_4·2H_2O$ and $Ca(HC_2O_4)_2$, as presented in Eqs. (8–9) (Ma et al., 2019). A higher pH value resulted in a higher Al/Si concentration ratio (C_{Al}/C_{Si} ratio) as plotted in Fig. 3c, but the high pH (> 4.0) caused a lower retention of Al. As observed in Table 2, the concentration of Al in the leachate at pH 4.0 using $CaCO_3$ was maintained at 3965 mg/L (0.15 mol/L), close to original Fe-removed leachate. The findings suggested that the effective separation of Al, Si, and Ti was achieved with SiO_2 and $CaC_2O_4·2H_2O$ as the precipitated products. From Fig. 4c, SiO_2 and $CaC_2O_4·2H_2O$ were of mutual adhesion, with visible independent SiO_2 particles which differed from those obtained by using CaO. The independent SiO_2 and $CaC_2O_4·2H_2O$ were conducive to further separation. Therefore, using cheap and widely available powdered $CaCO_3$ could achieve the separation of Al, Si, and Ti from Fe-removed leachate.

$$CaCO_3 + H_2C_2O_4 + H_2O \rightarrow CaC_2O_4·2H_2O + CO_2(g) \quad (8)$$

$$CaCO_3 + 2H_2C_2O_4 \rightarrow Ca(HC_2O_4)_2 + CO_2(g) + H_2O \quad (9)$$

3.5. Al species and Si- and Ti- precipitation mechanisms

Fig. 5 shows the contour plots for the change in concentration of $C_2O_4^{2-}$ in the Fe-removed leachate with the addition of NaOH, CaO, and $CaCO_3$ and the XRD patterns of the precipitates. It can be seen from Fig. 5a that increasing pH to 8.0 required a large amount of NaOH without declining the $C_2O_4^{2-}$ concentration. By contrast, the increase in

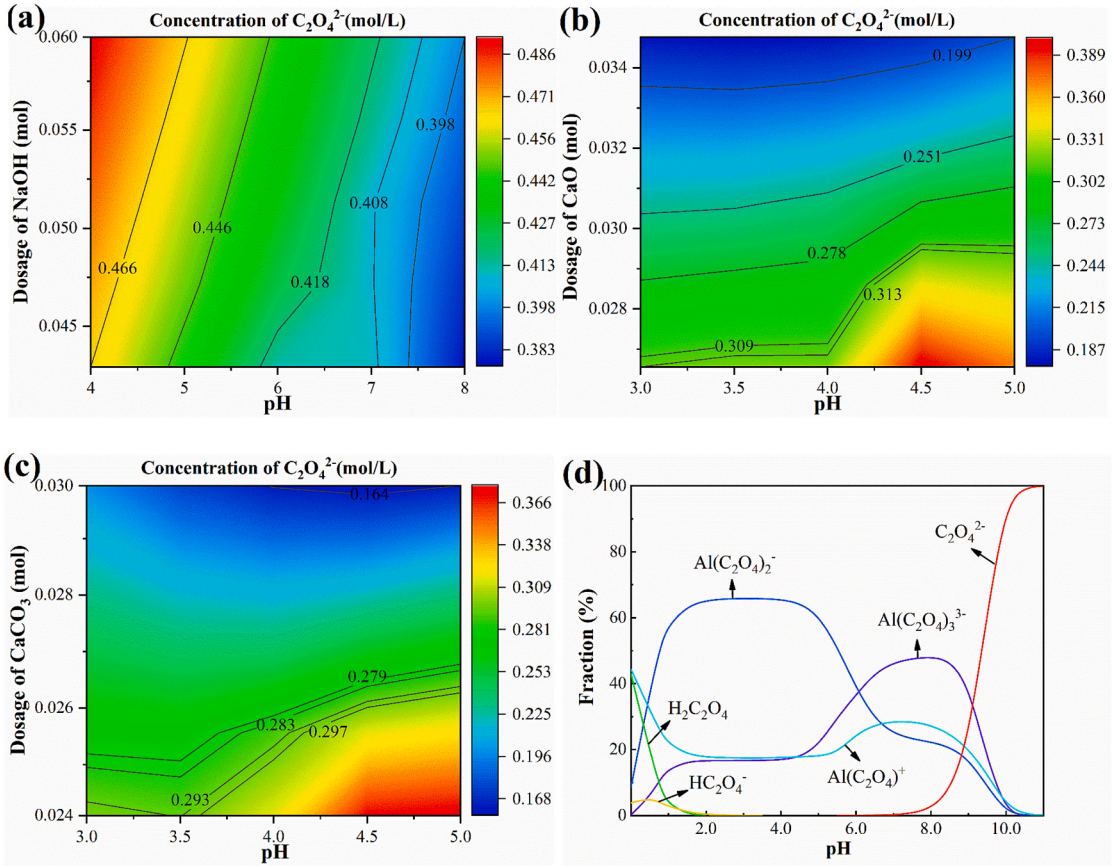

Fig. 5. Contour plots for concentration change of $C_2O_4^{2-}$ in the Fe-removed leachate with the addition of (a) NaOH, (b) CaO, and (c) $CaCO_3$. (d) The speciation diagrams of Al^{3+} in the oxalic acid medium with the addition of NaOH at 25 °C (thermodynamic data from the software Visual MINTEQ).

pH to 4.0 using CaO and $CaCO_3$ (Fig. 5b and c), caused a significant decrease in $C_2O_4^{2-}$ concentration and facilitated the precipitation of H_4SiO_4 at the pH range of 0.82–4.0. It was reported that pH and the presence of multivalent ions were the key solution parameters that influence Si speciation (Kambalina et al., 2014). It is worth noting that $C_2O_4^{2-}$ ion as a bidentate anionic ligand with a strong coordination effect could provide two pairs of electrons to metal ions (Chen et al., 2022). Various complexes between $C_2O_4^{2-}$ and Al^{3+}, such as $Al(C_2O_4)_2^-$ and $Al(C_2O_4)_3^{3-}$, have been formed in the oxalic acid medium (Liu et al., 2020). Cations (such as Al^{3+}) in the solution could reduce the solubility of SiO_2 and increase the precipitation efficiency of SiO_2 (Wang et al., 2021). After adding CaO and $CaCO_3$, Ca^{2+} combined with $C_2O_4^{2-}$ and precipitated so that decomplexation of $C_2O_4^{2-}$ and Al^{3+} occurred, resulting in Al^{3+} remaining in the leachate. Consequently, the concentration and speciation variation of Al^{3+} might affect the pH range of Si precipitation in the leachate.

In addition, the speciation of Al^{3+} in the oxalic acid leachate was calculated using the chemical equilibrium model software Visual MINTEQ, and the results are presented in Fig. 5d. As the initial leachate pH was increased from 0.8 to 2.0, $H_2C_2O_4$ was ionized to $HC_2O_4^-$ and $C_2O_4^{2-}$, and Al^{3+} was complexed with $C_2O_4^{2-}$. At pH of 2.0–5.0, Al^{3+} existed mainly as $Al(C_2O_4)_2^-$ and subsequently changed to $Al(C_2O_4)_2^-$, Al $(C_2O_4)_3^{3-}$ and $AlC_2O_4^+$ at pH of 5.0–6.5. The phenomena that the retention efficiencies of Si and Ti decreased significantly were indeed observed at the pH range of 5.0–6.5 (Fig. 3a). Therefore, the concentration and speciation variations of Al^{3+} are the main reason for the successful precipitation of Si and Ti in the leachate.

3.6. The primary products

3.6.1. The primary product of Si and Ti

The independent SiO_2 and $CaC_2O_4{\cdot}2H_2O$ particles were generated as precipitated solids in the Fe-removed leachate by adding $CaCO_3$ to adjust pH from 0.8 to 4.0. The data in Table 3 demonstrated that the filtered precipitate contained 12.7% SiO_2 and 2.8% TiO_2. The major component of the precipitate, $CaC_2O_4{\cdot}2H_2O$ could be thermally decomposed to $CaCO_3$ after roasting at 520 °C (Bushuev and Zinin, 2016; Li et al., 2022a). Subsequently, the wash process of roasted precipitate with dilute HCl was employed to remove $CaCO_3$ and to minimize the loss of Si and Ti. From the SEM and XRF analysis of the precipitate (Fig. 6 and Table 3), a porous amorphous Ti-rich SiO_2 primary product was obtained, in which the contents of the SiO_2 and TiO_2 reached 70.8 and 9.4%, respectively.

Additionally, the roasted precipitate can be recycled as $CaCO_3$ for pH

Table 3
Compositions of the precipitates after adding $CaCO_3$, roasting, and washing after 3 experimental cycles.

Content (wt%)	Al_2O_3	SiO_2	CaO	TiO_2	Na_2O	Fe_2O_3	MgO	K_2O	LOI
Precipitate using $CaCO_3$ pH of 4.0	1.20	12.7	26.8	2.79	0.29	0.11	0.07	0.15	54.8
Roasted precipitate	1.75	18.6	43.7	4.34	0.61	0.17	0.10	0.24	29.2
HCl washed precipitate	2.94	70.8	3.69	9.44	0.62	0.23	0.19	0.61	10.5

Based on XRF; LOI is loss on ignition.

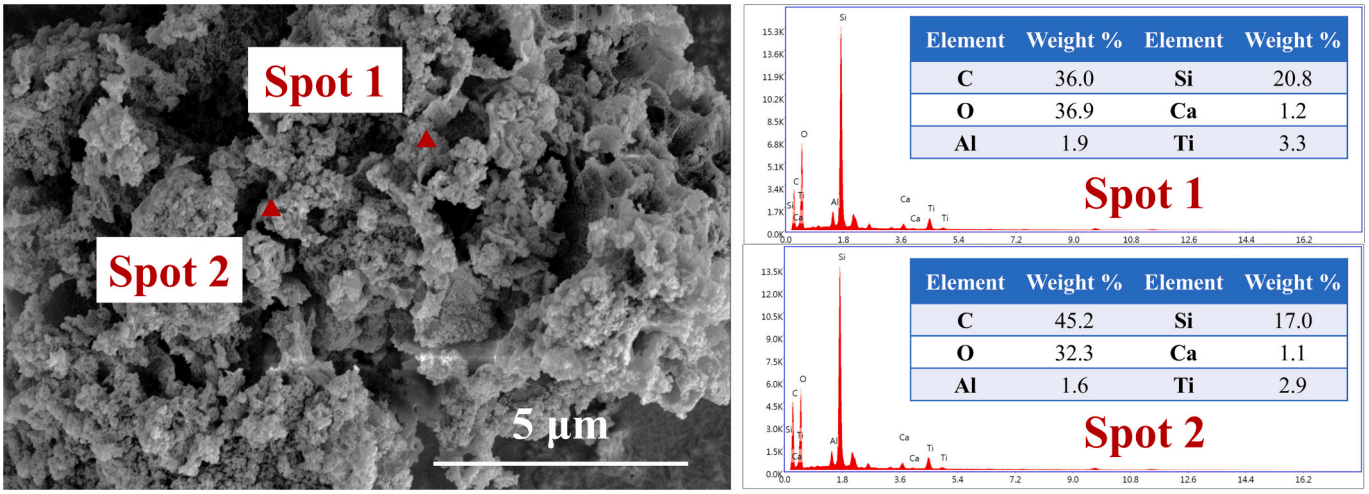

Fig. 6. SEM and EDS analyses of the HCl washed precipitate (Ti-rich SiO_2 primary product).

Table 4
The element contents in precipitates of the cycling process determined by EDS elemental mapping analysis.

Content (wt%)	Si	Ca	Ti	Si/Ca	Ti/Ca	C	O
Cycling-0	4.5	32.4	1.8	0.14	0.06	12.7	48.6
Cycling-1	11.5	20.7	3.4	0.56	0.16	13.1	51.4
Cycling-2	12.1	15.0	3.9	0.81	0.26	20.1	48.9
Cycling-3	21.3	8.3	6.3	2.57	0.76	17.7	46.4

adjustment and this recycling process was investigated in this trial. From the data of the surface scan shown in Table 4 and Fig. S1, the Si/Ca ratio raised from 0.14 to 2.57, and the Ti/Ca ratio raised from 0.06 to 0.76 in the precipitates after 3 experimental cycles. The Si/Ca ratio and Ti/Ca ratio in the newly generated precipitates gradually increased. Accordingly, this recycling process could minimize the required amount of fresh $CaCO_3$. The recycling process was of economic and environmental benefits, and can also further enrich the Si and Ti in the precipitation.

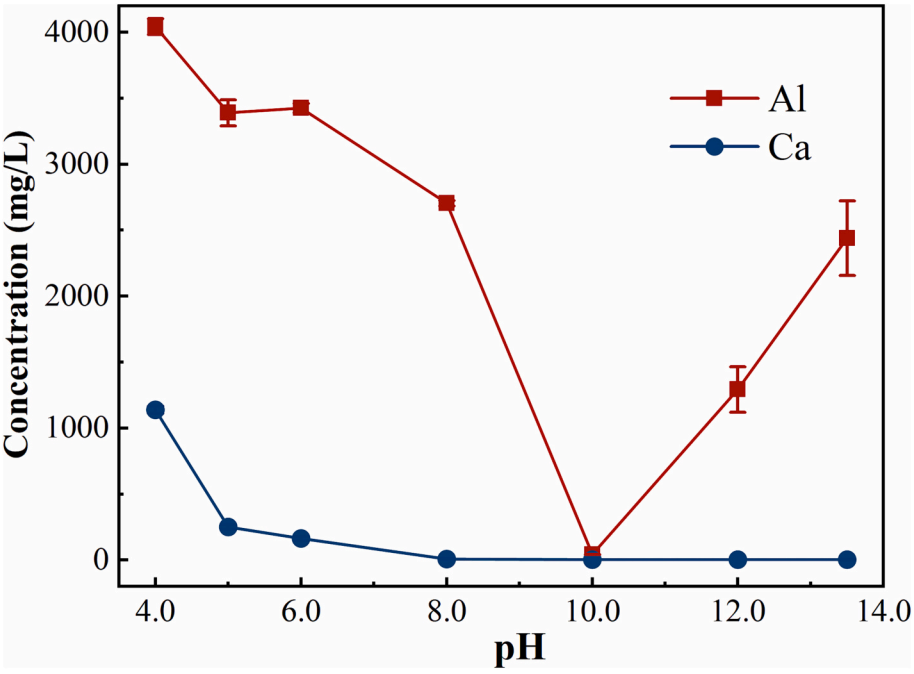

Fig. 7. Concentration variations of Al and Ca in the Al-enriched leachate with the addition of NaOH.

Table 5
The chemical compositions of precipitates obtained at different pH stages.

Content (wt%)	Al_2O_3	SiO_2	CaO	TiO_2	Na_2O	TFe_2O_3	MgO	K_2O	LOI
pH = 4.0–10.0	35.4	3.81	8.29	0.28	1.37	1.45	1.44	0.14	48.1
pH = 5.0–10.0	41.2	0.77	5.42	0.02	1.12	1.68	1.63	0.08	47.7
pH = 6.0–10.0	45.3	0.87	1.56	0.09	2.43	1.83	2.20	0.16	45.9

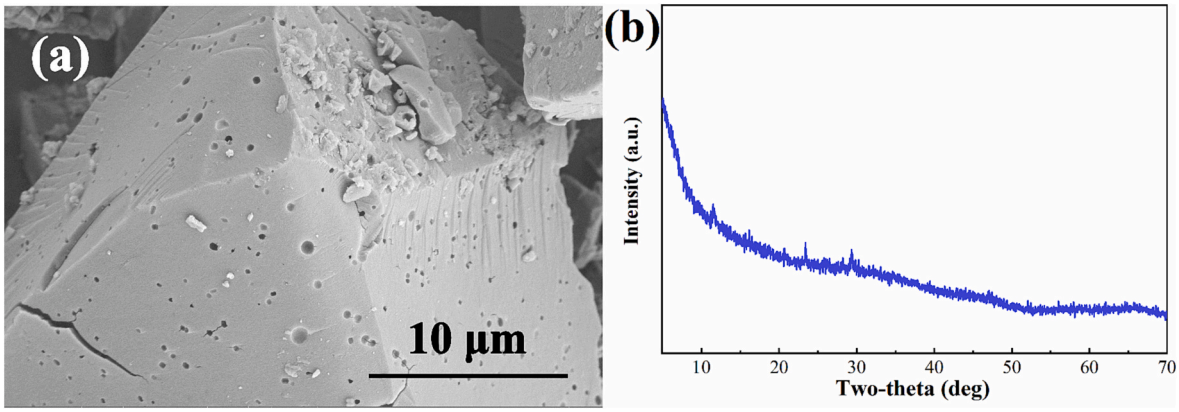

Fig. 8. (a) SEM image and (b) XRD pattern of the $Al(OH)_3$ primary product.

3.6.2. The primary product of $Al(OH)_3$

The Al-enriched leachate was obtained after the pH of the Fe-removed leachate was increased to 4.0 using $CaCO_3$. The major elements in the Al-enriched leachate were Al^{3+}, Na^{+}, and the newly introduced Ca^{2+} as shown in Eq. (9) and Table 2. The purpose of NaOH addition into the Al-enriched leachate was to separate the Al^{3+} forming $Al(OH)_3$ primary product. To obtain the maximum Al recovery and to save NaOH dosage, the variations of Al and Ca concentrations were investigated as illustrated in Fig. 7. At pH >10.0, $Al(OH)_3$ gradually redissolved as $Al(OH)_4^-$ which was characteristic of the amphoteric hydroxide (Peng et al., 2014; Narayanan et al., 2017). Table 5 shows that the content of impurity Ca reached 8.3% (as oxides) and Al reached 35.4% when the pH of the Al-enriched leachate was adjusted directly from 4.0 to 10.0 with NaOH. It is concluded that Ca in the Al-enriched leachate influenced the purity of the $Al(OH)_3$ primary product and must be removed before $Al(OH)_3$ precipitation. In this context, Ca can be removed at pH of 5.0 or 6.0 by adding NaOH.

The pH of the Al-enriched leachate was then adjusted from 6.0 to 10.0 when high purity of the $Al(OH)_3$ product could be attained. Meanwhile, the purity of the $Al(OH)_3$ primary product achieved 45.3%, and the LOI of the $Al(OH)_3$ primary product reached 45.9% which was considered as the content of the water of crystallization. The $Al(OH)_3$ primary product was made up of irregular massive particles as shown in Fig. 8a and demonstrated to be amorphous colloids without principal fingerprint peaks of $Al(OH)_3$ found in the XRD pattern (Fig. 8b). High purity amorphous $Al(OH)_3$ can be used to purify wastewater and as a precursor to manufacture aluminum products (Wang et al., 2012; Baccarella et al., 2021). Additionally, the filtrate at pH 10.0 contained few impurities and could be recycled for the preparation of $Al(OH)_3$ (Table S1). Therefore, high purity amorphous $Al(OH)_3$ primary product can be obtained after Ca-removal and precipitation process, which extracts more value from the Fe-removed leachate of RM.

4. Conclusions

The oxalic acid leaching process of Fe from RM using 1.0 mol/L oxalic acid, L/S ratio of 15 mL/g, at 80 °C over 2 h co-dissolved Al, Si, and Ti. The leaching efficiencies of Al, Si, and Ti from RM could achieve 63.5, 73.9, and 75.6%, respectively. Adding NaOH to adjust pH to 8.0 could remove Si and Ti from the Fe-removed leachate but Al suffered great losses. The use of CaO to adjust pH to pH 4.0 could precipitate a mixture of Ca_2SiO_4 and $CaC_2O_4{\cdot}2H_2O$. However, the addition of $CaCO_3$ to adjust pH to 4.0 exhibited a fast reaction with $C_2O_4^{2-}$ and generated mixed precipitates of SiO_2 and $CaC_2O_4{\cdot}2H_2O$. The $CaCO_3$ addition is a sustainable approach with minimum waste generation and reagent consumption by recirculation of $CaC_2O_4{\cdot}2H_2O$. Finally, Ti-rich SiO_2 (70.8% SiO_2, 9.4% TiO_2) and $Al(OH)_3$ were obtained as primary products. The findings of this study provide a method for recovery of Al, Si, and Ti from the RM-oxalic acid leaching process, and present a significant contribution to the understanding of the separation behaviors of Al, Si, and Ti in the Fe-removed oxalic acid leachate.

CRediT authorship contribution statement

Wanyan Li: Investigation, Methodology, Data curation, Validation, Writing – original draft. **Ning Wang:** Conceptualization, Resources, Supervision. **Fanghai Lu:** Resources. **Hongyun Chai:** Supervision. **Hannian Gu:** Writing – review & editing, Conceptualization, Resources, Supervision, Funding acquisition.

Declaration of Competing Interest

The authors declare that they have no known competing financial interests or personal relationships that could have appeared to influence the work reported in this paper.

Acknowledgments

The work was financially supported by the National Natural Science Foundation of China (U1812402), the Youth Innovation Promotion Association CAS (2021400), Guizhou Outstanding Young Scientific and Technological Talents Project (2021-5641), and Guizhou Provincial Science and Technology Project (2023-243).

Appendix A. Supplementary data

Supplementary data to this article can be found online at https://doi.org/10.1016/j.hydromet.2023.106221.

References

Agrawal, S., Dhawan, N., 2020. Investigation of carbothermic microwave reduction followed by acid leaching for recovery of iron and aluminum values from Indian red mud. Miner. Eng. 159, 106653 https://doi.org/10.1016/j.mineng.2020.106653.

Agrawal, S., Dhawan, N., 2021. Evaluation of red mud as a polymetallic source - a review. Miner. Eng. 171, 107084 https://doi.org/10.1016/j.mineng.2021.107084.

Agrawal, S., Dhawan, N., 2022. Process flowsheet for extraction of Fe, Al, Ti, Sc, and Ga values from red mud. Miner. Eng. 184, 107601 https://doi.org/10.1016/j.mineng.2022.107601.

Ambikadevi, V.R., Lalithambika, M., 2000. Effect of organic acids on ferric iron removal from iron-stained kaolinite. Appl. Clay Sci. 16, 133–145. https://doi.org/10.1016/S0169-1317(99)00038-1.

Baccarella, A.M., Garrard, R., Beauvais, M.L., Bednarksi, U., Fischer, S., Abeykoon, A.M. M., Chapman, K.W., Phillips, B.L., Parise, J.B., Simonson, J.W., 2021. Cluster mediated conversion of amorphous $Al(OH)_3$ to γ-AlOOH. J. Solid State Chem. 301, 122340 https://doi.org/10.1016/j.jssc.2021.122340.

Barca, C., Magari, M., Miche, H., Hennebert, P., 2022. Effect of different wastewater composition on kinetics, capacities, and mechanisms of phosphorus sorption by carbonated bauxite residue. J. Environ. Chem. Eng. 10, 108922 https://doi.org/10.1016/j.jece.2022.108922.

Borra, C.R., Blanpain, B., Pontikes, Y., Binnemans, K., Gerven, T.V., 2016. Recovery of rare earths and other valuable metals from bauxite residue (red mud): a review. J. Sustain. Metal. 2, 365–386. https://doi.org/10.1007/s40831-016-0068-2.

Bushuev, N.N., Zinin, D.S., 2016. Thermal decomposition features of calcium and rare-earth oxalates. Russ. J. Inorg. Chem. 61 (2), 161–167. https://doi.org/10.1134/S0036023616020030.

Chen, H., Ren, B., Liu, M., Qin, T., Guo, Q., Li, G., Gong, D., Cheng, G., Chen, J., Li, B., 2022. Facile synthesis of hydroxyl aluminum oxalate based on the hydrothermal reaction of boehmite and oxalic acid. Colloids Surf. A Physicochem. Eng. Asp. 639, 128344 https://doi.org/10.1016/j.colsurfa.2022.128344.

Deng, B., Li, G., Luo, J., Ye, Q., Liu, M., Peng, Z., Jiang, T., 2017. Enrichment of Sc_2O_3 and TiO_2 from bauxite ore residues. J. Hazard. Mater. 331, 71–80. https://doi.org/10.1016/j.jhazmat.2017.02.022.

Gräfe, M., Power, G., Klauber, C., 2011. Bauxite residue issues: III. Alkalinity and associated chemistry. Hydrometallurgy 108, 60–79. https://doi.org/10.1016/j.hydromet.2011.02.004.

Gu, H., Hargreaves, J.S.J., Jiang, J., Rico, J.L., 2017. Potential routes to obtain value-added iron-containing compounds from red mud. J. Sustain. Metal. 3 (3), 561–569. https://doi.org/10.1007/s40831-016-0112-2.

Habibi, H., Piruzian, D., Shakibania, S., Pourkarimi, Z., Mokmeli, M., 2021. The effect of carbothermal reduction on the physical and chemical separation of the red mud components. Miner. Eng. 173, 107216 https://doi.org/10.1016/j.mineng.2021.107216.

Huang, Y., Chai, W., Han, G., Wang, W., Yang, S., Liu, J., 2016. A perspective of stepwise utilisation of Bayer red mud: step two-extracting and recovering Ti from Ti-enriched tailing with acid leaching and precipitate flotation. J. Hazard. Mater. 307, 318–327. https://doi.org/10.1016/j.jhazmat.2016.01.010.

Huang, Q., Huang, K., Lu, Y., Liu, Y., Xiong, H., Dong, H., 2021. Recovery of iron and aluminum from red mud by oxalic acid leaching and solar photocatalysis. Environ. Eng. 39 (12), 199–205 (In Chinese). 10.13205/j.hjgc.202112030.

Kambalina, M., Mazurova, I., Skvortsova, L., Guseva, N., An, V., 2014. Study of aqueous chemical forms of silicon in organic-rich waters. Proc. Chem. 10, 36–42. https://doi.org/10.1016/j.proche.2014.10.008.

Kong, X., Li, M., Xue, S., Hartley, W., Chen, C., Wu, C., Li, X., Li, Y., 2017. Acid transformation of bauxite residue: conversion of its alkaline characteristics. J. Hazard. Mater. 324, 382–390. https://doi.org/10.1016/j.jhazmat.2016.10.073.

Lee, M., Saunders, J.A., 2003. Effects of pH on metals precipitation and sorption. Vadose Zone J. 2 (2), 177–185. https://doi.org/10.2136/vzj2003.1770.

Li, W., Yan, X., Niu, Z., Zhu, X., 2021. Selective recovery of vanadium from red mud by leaching with using oxalic acid and sodium sulfite. J. Environ. Chem. Eng. 9 (4), 105669 https://doi.org/10.1016/j.jece.2021.105669.

Li, W., Li, Z., Wang, N., Gu, H., 2022a. Selective extraction of rare earth elements from red mud using oxalic and sulfuric acids. J. Environ. Chem. Eng. 10 (6), 108650 https://doi.org/10.1016/j.jece.2022.108650.

Li, Z., Gu, H., Hong, B., Wang, N., Chen, M., 2022b. An innovative process for dealkalization of red mud using leachate from Mn-containing waste. J. Environ. Chem. Eng. 10 (2), 107222 https://doi.org/10.1016/j.jece.2022.107222.

Liu, Z., Li, H., 2015. Metallurgical process for valuable elements recovery from red mud-a review. Hydrometallurgy 155, 29–43. https://doi.org/10.1016/j.hydromet.2015.03.018.

Liu, Y., Naidu, R., 2014. Hidden values in bauxite residue (red mud): recovery of metals. Waste Manag. 34, 2662–2673. https://doi.org/10.1016/j.wasman.2014.09.003.

Liu, Z., Huang, J., Zhang, Y., Liu, H., Luo, D., 2020. Separation and recovery of vanadium and aluminum from oxalic acid leachate of shale by solvent extraction with Aliquat 336. Sep. Purif. Technol. 249, 116867 https://doi.org/10.1016/j.seppur.2020.116867.

Liu, X., Han, Y., He, F., Gao, P., Yuan, S., 2021. Characteristic, hazard and iron recovery technology of red mud-a critical review. J. Hazard. Mater. 420, 126542 https://doi.org/10.1016/j.jhazmat.2021.126542.

Liu, Z., Sheng, M., He, Y., Zhou, H., Huang, J., Luo, X., Zhang, Y., 2022. Coordination mechanism of aluminum with oxalate and fluoride in aluminum crystallization from vanadium extraction wastewater. J. Mol. Liq. 347, 117992 https://doi.org/10.1016/j.molliq.2021.117992.

Lyu, F., Hu, Y., Wang, L., Sun, W., 2021. Dealkalization processes of bauxite residue: a comprehensive review. J. Hazard. Mater. 403, 123671 https://doi.org/10.1016/j.jhazmat.2020.123671.

Ma, Q., Liu, C., Ma, J., Chu, B., He, H., 2019. A laboratory study on the hygroscopic behavior of $H_2C_2O_4$-containing mixed particles. Atmos. Environ. 200, 34–39. https://doi.org/10.1016/j.atmosenv.2018.11.056.

Milne, N.A., O'Reilly, T., Sanciolo, P., Ostarcevic, E., Beighton, M., Taylor, K., Mullett, M., Tarquin, A.J., Gray, S.R., 2014. Chemistry of silica scale mitigation for RO desalination with particular reference to remote operations. Water Res. 65, 107–133. https://doi.org/10.1016/j.watres.2014.07.010.

Narayanan, R., Kazantzis, N.K., Emmert, M.H., 2017. Selective process steps for the recovery of scandium from Jamaican bauxite residue (red mud). ACS Sustain. Chem. Eng. 6 (1), 1478–1488. https://doi.org/10.1021/acssuschemeng.7b03968.

Panda, S., Costa, R.B., Shah, S.S., Mishra, S., Akcil, A., 2021. Biotechnological trends and market impact on the recovery of rare earth elements from bauxite residue (red mud)-a review. Resour. Conserv. Recycl. 171, 105645 https://doi.org/10.1016/j.resconrec.2021.105645.

Peng, J., Wang, X., Jiang, C., Wang, M., Ma, Y., Xiang, X., 2014. Separation of Mo(VI) and Fe(III) from the acid leaching solution of carbonaceous Ni-Mo ore by ion exchange. Hydrometallurgy 142 (1), 116–120. https://doi.org/10.1016/j.hydromet.2013.11.014.

Pepper, R.A., Couperthwaite, S.J., Millar, G.J., 2016. Comprehensive examination of acid leaching behaviour of mineral phases from red mud: recovery of Fe, Al, Ti, and Si. Miner. Eng. 99, 8–18. https://doi.org/10.1016/j.mineng.2016.09.012.

Qu, Y., Li, H., Shi, B., Gu, H., Yan, G., Liu, Z., Luo, R., 2022. Bioleaching performance of titanium from bauxite residue under a continuous mode using Penicillium tricolor. Bull. Environ. Contam. Toxicol. 109, 61–67. https://doi.org/10.1007/s00128-022-03518-2.

Rivera, R.M., Ulenaers, B., Ounoughene, G., Binnemans, K., Gerven, T.V., 2018. Extraction of rare earths from bauxite residue (red mud) by dry digestion followed by water leaching. Miner. Eng. 119, 82–92. https://doi.org/10.1016/j.mineng.2018.01.023.

Taneez, M., Hurel, C., 2019. A review on the potential uses of red mud as amendment for pollution control in environmental media. Environ. Sci. Pollut. Res. 26, 22106–22125. https://doi.org/10.1007/s11356-019-05576-2.

Tanvar, H., Mishra, B., 2021. Hydrometallurgical recycling of red mud to produce materials for industrial applications: alkali separation, iron leaching and extraction. Metall. Mater. Trans. B Process Metall. Mater. Process. Sci. 52, 2021–3543. https://doi.org/10.1007/s11663-021-02285-5.

Ujaczki, É., Courtney, R., Cusack, P., Chinnam, R.K., Clifford, S., Curtin, T., O'Donoghue, L., 2019. Recovery of gallium from bauxite residue using combined oxalic acid leaching with adsorption onto zeolite HY. J. Sustain. Metal. 5, 262–274. https://doi.org/10.1007/s40831-019-00226-w.

Wan, J., Chen, T., Zhou, X., Luo, Y., Liu, W., Lu, Q., 2021. Efficient improvement for the direct reduction of high-iron red mud by co-reduction with high-manganese iron ore. Miner. Eng. 174, 107024 https://doi.org/10.1016/j.mineng.2021.107024.

Wang, W., Zhang, X., Wang, H., Wang, X., Zhou, L., Liu, R., Liang, Y., 2012. Laboratory study on the adsorption of Mn^{2+} on suspended and deposited amorphous $Al(OH)_3$ in drinking water distribution systems. Water Res. 46, 4063–4070. https://doi.org/10.1016/j.watres.2012.05.017.

Wang, W., Geilert, S., Wei, H., Jiang, S., 2021. Competition of equilibrium and kinetic silicon isotope fractionation during silica precipitation from acidic to alkaline pH solutions in geothermal systems. Geochim. Cosmochim. Acta 306, 44–62. https://doi.org/10.1016/j.gca.2021.05.022.

Wilhelm, S., Kind, M., 2015. Influence of pH, temperature and sample size on natural and enforced syneresis of precipitated silica. Polymers 7, 2504–2521. https://doi.org/10.3390/polym7121528.

Xue, S., Wu, Y., Li, Y., Kong, X., Zhu, F., William, H., Li, X., Ye, Y., 2019. Industrial wastes applications for alkalinity regulation in bauxite residue: a comprehensive review. J. Cent. South Univ. 26, 268–288. https://doi.org/10.1007/s11771-019-4000-3.

Yang, Y., Wang, X., Wang, M., Wang, H., Xian, P., 2015. Recovery of iron from red mud by selective leach with oxalic acid. Hydrometallurgy 157, 239–245. https://doi.org/10.1016/j.hydromet.2015.08.021.

Yang, Y., Wang, X., Wang, M., Wang, H., Xian, P., 2016. Iron recovery from the leached solution of red mud through the application of oxalic acid. Int. J. Miner. Process. 157, 145–151. https://doi.org/10.1016/j.minpro.2016.11.001.

Yu, Z., Shi, Z., Chen, Y., Niu, Y., Wang, Y., Wan, P., 2012. Red-mud treatment using oxalic acid by UV irradiation assistance. Trans. Nonferrous Metals Soc. China 22 (2), 456–460. https://doi.org/10.1016/S1003-6326(11)61198-9.

Yu, J., Li, Y., Lv, Y., Han, Y., Gao, P., 2022. Recovery of iron from high-iron red mud using suspension magnetization roasting and magnetic separation. Miner. Eng. 178, 107394 https://doi.org/10.1016/j.mineng.2022.107394.

Zhang, Y., Qian, W., Zhou, P., Liu, Y., Lei, X., Li, B., Ning, P., 2021. Research on red mud-limestone modified desulfurization mechanism and engineering application. Sep. Purif. Technol. 272, 118867.

Zhou, G., Wang, Y., Qi, T., Zhou, Q., Liu, G., Peng, Z., Li, X., 2023. Toward sustainable green alumina production: a critical review on process discharge reduction from gibbsitic bauxite and large-scale applications of red mud. J. Environ. Chem. Eng. 11, 109433 https://doi.org/10.1016/j.jece.2023.109433.

Zhu, X., Li, W., Guan, X., 2015. Kinetics of titanium leaching with citric acid in sulfuric acid from red mud. Trans. Nonferrous Metals Soc. China 25 (9), 3139–3145. https://doi.org/10.1016/S1003-6326(15)63944-9.